Journal of Pharmaceutical Analysis 12 (2022) 808–813

Contents lists available at ScienceDirect

Journal of Pharmaceutical Analysis

journal homepage: www.elsevier.com/locate/jpa

Original article

Sensitive detection of microRNAs using polyadenine-mediated fluorescent spherical nucleic acids and a microfluidic electrokinetic signal amplification chip

Jun Xu [a], Qing Tang [a], Runhui Zhang [a], Haoyi Chen [b], Bee Luan Khoo [c], Xinguo Zhang [a], Yue Chen [a], Hong Yan [a], Jincheng Li [a], Huaze Shao [a], Lihong Liu [a, *]

[a] NMPA Key Laboratory for Research and Evaluation of Drug Metabolism, Guangdong Provincial Key Laboratory of New Drug Screening, School of Pharmaceutical Sciences, Southern Medical University, Guangzhou, 510515, China
[b] The Second Clinical Medical School, Southern Medical University, Guangzhou, 510515, China
[c] Department of Biomedical Engineering, City University of Hong Kong, Hong Kong, 999077, China

ARTICLE INFO

Article history:
Received 5 February 2022
Received in revised form
24 May 2022
Accepted 27 May 2022
Available online 1 June 2022

Keywords:
MicroRNAs
Microfluidic chip
Electrokinetic signal amplification
Polyadenine-DNA
Gold nanoparticle

ABSTRACT

The identification of tumor-related microRNAs (miRNAs) exhibits excellent promise for the early diagnosis of cancer and other bioanalytical applications. Therefore, we developed a sensitive and efficient biosensor using polyadenine (polyA)-mediated fluorescent spherical nucleic acid (FSNA) for miRNA analysis based on strand displacement reactions on gold nanoparticle (AuNP) surfaces and electrokinetic signal amplification (ESA) on a microfluidic chip. In this FSNA, polyA-DNA biosensor was anchored on AuNP surfaces via intrinsic affinity between adenine and Au. The upright conformational polyA-DNA recognition block hybridized with 6-carboxyfluorescein-labeled reporter-DNA, resulting in fluorescence quenching of FSNA probes induced by AuNP-based resonance energy transfer. Reporter DNA was replaced in the presence of target miRNA, leading to the recovery of reporter-DNA fluorescence. Subsequently, reporter-DNAs were accumulated and detected in the front of with Nafion membrane in the microchannel by ESA. Our method showed high selectivity and sensitivity with a limit of detection of 1.3 pM. This method could also be used to detect miRNA-21 in human serum and urine samples, with recoveries of 104.0%–113.3% and 104.9%–108.0%, respectively. Furthermore, we constructed a chip with three parallel channels for the simultaneous detection of multiple tumor-related miRNAs (miRNA-21, miRNA-141, and miRNA-375), which increased the detection efficiency. Our universal method can be applied to other DNA/RNA analyses by altering recognition sequences.

1. Introduction

Cancer mortality has significantly increased in the recent years and approximately 10 million deaths have been reported worldwide each year [1]. An early cancer diagnosis system is critical for patient survival. Biomarker-based cancer diagnostic tests can significantly improve early detection and subsequent treatment strategies [2]. MicroRNAs (miRNAs) are a class of small endogenous RNA molecules of approximately 20–24 nucleotides that play important roles as post-transcriptional regulators of gene expression [3]. Recently, aberrant miRNA expression was found to be implicated in the development of several cancers, including colorectal [4], lung [5], breast [6], and prostate [7] cancers. Thus, miRNAs are potentially promising biomarkers of cancer that can be used in the early diagnostics and monitoring of various tumors.

Considering the clinical relevance of miRNAs, several analytical methods have been developed. Northern blotting robustly detects miRNAs; however, this technique is restricted by the low sensitivity, labor intensiveness, and long duration [8]. Microarrays, reverse transcription quantitative polymerase chain reaction, and RNA sequencing are widely used because of their excellent analytical performances [9]. However, these methods generally involve tedious sample processing methods and expensive equipment or lack sensitivity. miRNAs are typically present in trace amounts and are present in varying concentrations in

Peer review under responsibility of Xi'an Jiaotong University.
* Corresponding author.
E-mail address: lhliu@smu.edu.cn (L. Liu).

https://doi.org/10.1016/j.jpha.2022.05.009

different biological fluids. Moreover, they are implicated in cancer development. Therefore, a cost-effective, sensitive, and rapid assay for measuring miRNA levels in different biological samples is warranted.

In recent decades, gold nanoparticle (AuNP)-based fluorescent spherical nucleic acid (FSNA) probes have garnered considerable attention in biosensor research due to their high sensitivity and selectivity, large surface area, and low toxicity [10–12]. Although the Au-thiol connection strategy has been certified to be useful in the fabrication of FSNA, it is limited by the total number and conformation of surface-tethered DNA molecules. These factors affect hybridization and specific DNA-Au binding [13–15]. Previous studies have reported that polyadenine (polyA) sequences have a high affinity for AuNP surfaces [16–18]. Pei et al. [14] proposed a salt-aging strategy for preparing FSNA with modification-free, diblock DNA oligonucleotides. In addition, they demonstrated that polyA sequences provide anchoring stability and can form an upright conformation, which facilitates DNA hybridization through the elimination of nonspecific binding. However, this salt-aging method requires approximately 3 days; moreover, the salt concentrations must be controlled to avoid AuNP aggregation. A recent study reported a novel FSNA freezing-based labeling strategy. This method involves a single step, does not include salt-aging or thiols, and is less time-consuming and more cost-effective than the salt-aging method [19]. Because of these characteristics, the freezing-based labeling strategy has shown significant potential for diverse biosensor targeting, including miRNAs.

Microfluidic chips are miniaturized, portable, and cost-effective entities that are widely used to detect disease-related biomarkers [20]. For example, Yang et al. [21] reported an exosome capture and relevant RNA detection method for non-small cell lung cancer diagnostics based on cationic lipoplex NPs in a microfluidic device. Gao et al. [22] developed a surface-enhanced Raman spectroscopy-assisted pump-free microfluidic immunoassay for prostate cancer screening, which showed excellent specificity and sensitivity. In recent years, with increasing development in nanoscience, micro-nanofluidic systems combined with different nanostructures have become topical. These novel nanofluidic devices can pre-concentrate samples more efficiently than pure microfluidic devices because of their ion concentration polarization (ICP) abilities [23,24]. Microfluidic chips with ICP-based electrokinetic signal amplification (ESA) have been extensively studied for diverse charged biomolecules and were found to display high sensitivity, indicating that this is a promising method of detection of trace analytes [25,26]. Moreover, multi-channels can be easily fabricated on one chip and can simultaneously and efficiently determine multiple targets.

Considering these advantages, we fabricated a biosensor system that detects miRNAs in a sensitive and specific manner by combining FSNA biosensor and ESA chip (FSNA-ESA) technology. This method can sensitively detect miRNAs in serum and urine matrix within 30 min. Additionally, the simultaneous detections of multibiomarkers improved diagnostic accuracy, increased detection efficiency, and reduced costs [27]. To this end, we further developed a method for the detection of multiple miRNAs (miRNA-21, miRNA-141, and miRNA-375 that are highly expressed in prostate cancer [7]) in a specimen based on a three parallel channel (TPC) microfluidic chip.

2. Experimental

2.1. Materials

All oligonucleotides (Table S1 and the Supplementary data) and RNase inhibitors were supplied by Sangon Biotech Co., Ltd. (Shanghai, China). $HAuCl_4$ and sodium citrate were obtained from National Pharmaceutical Group Corporation (Beijing, China). Phosphate buffered saline (PBS; 1× PBS, pH 7.4) was supplied by Guangzhou Alexan Biotech Co., Ltd. (Guangzhou, China). Sodium chloride and platinum wire electrodes were purchased from Tianjin Fuchen Chemical Reagents Factory (Tianjin, China) and Xiya Chemical Technology Co., Ltd. (Linyi, China), respectively. Sylgrd 184 silicone elastomer polydimethylsiloxane (PDMS) and 20% (*m*/*m*) Nafion resin were provided by Dow Corning (Midland, MI, USA) and Sigma-Aldrich (Shanghai, China), respectively. Microfluidic chips were prepared using glass as a substrate, PDMS and curing agent were mixed (10:1, *m*/*m*) as a cover plate. All chemicals were of analytical grade and prepared in ultrapure water (18.2 MΩ·cm). Centrifuge tubes and pipette heads were autoclaved before use.

Direct current (DC) power (MP3001D, Maisheng, Dongguan, China) was used to supply DC voltages for microfluidic ESA. Fluorescence was recorded using an inverted fluorescence microscope (Leica DMIL LED, OSRAM GmbH, Wetzlar, Germany) equipped with a charge-coupled device camera (Leica DFC 360 FX) and images were quantified by free-software ImageJ. AuNPs and FSNAs were characterized using a Nanodrop 2000C spectrophotometer (Thermo Fisher Scientific Inc., Waltham, MA, USA), a Malvern Zetasizer Nano ZS instrument (Malvern, Melvin, UK), and transmission electron microscopy (TEM) (Hitachi, Ltd., Tokyo, Japan).

2.2. AuNP and FSNA synthesis

As previously reported, 13-nm AuNPs were synthesized using the sodium citrate reduction method [28]. Briefly, 1.7 mL of 1% $HAuCl_4$ and 48.3 mL of ultrapure water were added to a three-necked flask and boiled in an oil bath with stirring. Subsequently, 5 mL of 38.8 mM sodium citrate was rapidly added to the boiling solution. When the solution changed color from yellow to deep red (within approximately 15 min), the heating was stopped and the solution cooled to room temperature (25 °C) with stirring.

FSNAs were synthesized by the freezing-based labeling method. First, 2 μL (100 μM) of capture DNA sequence with polyA tails (polyA-DNA) was added to 100 μL of AuNP solution. This mixture was incubated at −20 °C for 2 h and then thawed. Second, 104 μL of buffer A (1× saline sodium citrate (SSC) pH 7.4 containing 150 mM NaCl and 17 mM phosphate) and 2 μL (100 μM) of reporter-DNA were added to the thawed solution and incubated for 30 min to form FSNAs. To remove free reporter-DNA, FSNAs were washed four times with buffer B (0.5× SSC pH 7.4 containing 75 mM NaCl and 8.5 mM phosphate) by centrifugation at 13,000 r/min at 4 °C for 15 min. Finally, FSNAs were dispersed in buffer B and stored at 4 °C in the dark.

AuNP and FSNAs preparation for TEM was performed as follows: FSNAs and AuNP solutions were diluted five times in ultrapure water, and 20 μL of aliquot was added to a TEM copper grid and air-dried for 5 min. TEM images were acquired on a Hitachi TEM at an operating voltage of 200 kV. AuNP and FSNAs characterization presented in Fig. S1 and the Supplementary data [29–31].

2.3. Microchip fabrication

The silicon mold substrate of the PDMS microchip was fabricated using standard soft lithography techniques. The ESA microchip contained one Nafion line and one PDMS chip with two parallel microchannels (width = 200 μm and height = 45 μm). A Nafion line was made using micro-flow patterning [32]. Briefly, 1.2 μL of Nafion resin was loaded into a PDMS mold, which had one 45-μm thick and 400-μm wide straight microchannel. Nafion resin was patterned on a glass substrate and followed the shape of the PDMS mold due to capillary forces. The PDMS mold was removed

and the Nafion line on the substrate solidified by heating at 95 °C for 3 min. Finally, this Nafion-patterned glass slide was irreversibly bonded to a PDMS chip after oxygen plasma treatment, and an H-shaped PDMS chip generated. The Nafion membrane was perpendicular to parallel microchannels, and reservoirs were constructed using 10-μL pipet tips inserted into reservoirs of the PDMS chip.

2.4. Sample preparation

To prepare samples for miRNA-21 detection, 20 μL of FSNA solution and 180 μL of different miRNA-21 concentrations were incubated in a 200-μL reaction system for 30 min at room temperature. After this, 6-carboxyfluorescein (6-FAM)-labeled reporter DNA in the solution was generated by centrifugation at 13,000 r/min for 15 min. The biological samples contained 1% serum or 1% urine. Samples for three-target detection were prepared as follows: three FSNA probes were designed according to miRNA-21, miRNA-141, and miRNA-375 sequences, and three targets were simultaneously detected in the TPC biochip.

3. Results and discussion

3.1. Principles of the FSNA-ESA system

An overview of the method principle is shown in Fig. 1. First, FSNAs were constructed using the freezing method based on intrinsic affinity between polyA-DNA sequences and the Au surface [16,19]. Second, 6-FAM-labeled reporter-DNA hybridized with the recognition polyA-DNA block, resulting in the fluorescence quenching of reporter-DNA via fluorescence resonance energy transfer [33]. Reporter DNA was replaced by a more efficient hybridization process between miRNAs and polyA-DNA in the presence of target miRNAs; thus, reporter-DNA fluorescence was restored. Finally, in an electric field, free reporter-DNAs accumulated on the front of the Nafion membrane due to Nafion ion selectivity [34]. In essence, reporter-DNAs were efficiently stacked by ESA on the biochip. Reporter-DNA fluorescence intensity was proportional to the miRNA concentration in biological samples and was used to quantitate the miRNA.

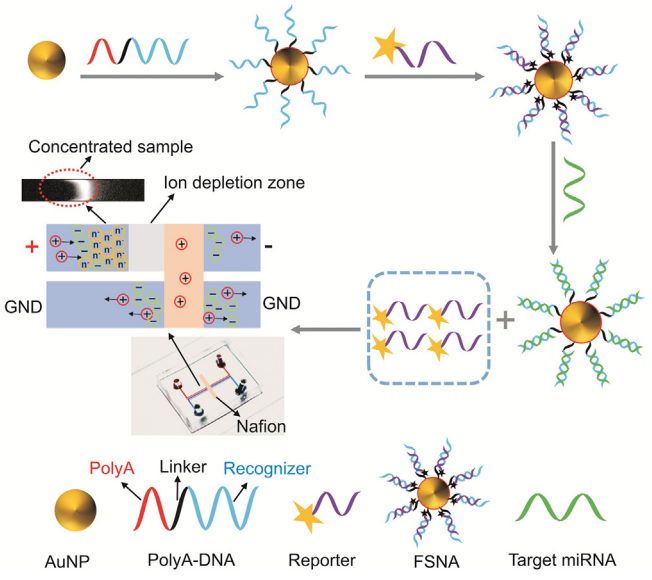

Fig. 1. Schematic illustration of the fluorescent spherical nucleic acids (FSNA)-electrokinetic signal amplification (ESA) system for miRNA detection. GND: ground; AuNP: gold nanoparticle; PolyA: polyadenine; miRNA: microRNA.

3.2. Optimization of polyA-DNA

The loading density of polyA-DNAs on AuNP surfaces could significantly affect FSNA sensitivity. To facilitate rapid and sensitive miRNA determination, polyA tail lengths of 10, 20, 30, and 40 nucleotides (nt) were investigated. PolyA 10-DNA showed failed labeling and was unable to protect AuNPs from aggregation (Fig. 2A). This might be due to a tendency to form secondary structures in recognition sequences, thus shielding A bases [19]. With increasing polyA lengths, the fluorescence intensity ($F–F_0$) was enhanced until polyA length reached 30 nt. However, fluorescent signal intensity decreased when polyA length increased to 40 nt. This was possibly due to fluorescence recovery in FSNA probes which were affected by DNA-capped AuNP density and related to polyA length. Thus, shorter polyA tails produced a higher surface density and steric hindrance, which led to inefficient hybridization. Moreover, longer polyA tails had a lower surface polyA-DNA density; therefore, reporter-DNA levels on AuNP surfaces were smaller [33] and generated lower fluorescence intensity. The ideal balance between surface density and reporter-DNA levels was achieved when polyA tail length was 30 nt; therefore, polyA 30 was selected for further studies.

Additionally, the fluorescence intensity enhanced with the increasing molar ratio between polyA-DNA and AuNP from 50:1 to 200:1, and reached a plateau when the molar ratio further increased (Fig. 2B). This was because polyA 30-DNA/AuNPs (200:1) provided enough sites to hybridize target miRNA-21; therefore, the 200:1 molar ratio was selected for further studies.

3.3. Optimizing buffer conditions

Buffer concentration is a key factor determining enrichment efficiency. In this study, PBS concentrations from 0.025× to 1× were investigated. As shown in Fig. 3A, fluorescence intensity increased when the PBS concentration was increased from 0.025× to 0.1×, but decreased when the concentration was greater than 0.1×. This result showed that the length of the depletion region (shown by the green arrow in Fig. 3A) decreased with the increased PBS concentration. Only a small number of cations in low concentration of PBS were pumped into the microchannel by electroosmotic flow (EOF). Negatively charged molecules had to move further toward the anodic reservoir and maintain electroneutrality at the depletion boundary. However, a mass of cations were contained in higher concentration PBS solution, so anionic analytes had to move slightly toward the anode. On one hand, the shorter depletion region formed a stronger electric field gradient distribution, which benefited the compression of fluorescence bands. On the other hand, higher ionic strength could destroy the electrical neutrality of the depletion zone and induce sample leakage, which was not conducive to reporter-DNA accumulation [26]. Therefore, 0.1× PBS was selected for further studies.

CH_3CN is commonly used as an additive for on-line sample preconcentration, which enables the rapid accumulation of reporter-DNAs via transient pseudo-isotachophoresis [35]. We investigated CH_3CN concentrations which ranged from 0% to 8% (V/V) in PBS. The fluorescence intensity of different CH_3CN concentrations after 30 min of ESA increased with the increased CH_3CN concentration of up to 3% (V/V), but then decreased at higher CH_3CN concentrations (Fig. 3B). This phenomenon was explained by the changing distribution of the electric field in the microchannel caused by CH_3CN, thereby improving the enrichment efficiency of ESA. However, excessive CH_3CN generated an EOF mismatch between sample and running buffer and led to low detection sensitivity. Therefore, 3% (V/V) CH_3CN was finally selected.

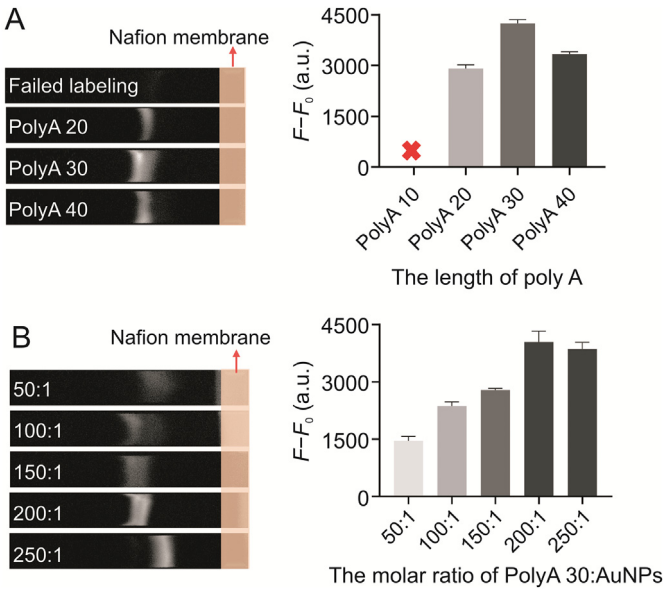

Fig. 2. (A) Effect of polyadenine (polyA) tail length on fluorescence intensity. (B) Effect of the molar ratio of polyA 30-DNA and gold nanoparticle (AuNP) on fluorescence intensity. F_0 and F are fluorescence intensities in the absence and presence of miRNA-21, respectively. Each point on the graph is the average value of three independent experiments. Conditions: 0.1× phosphate buffered saline (PBS) (pH 7.4, 3% (*V*/*V*) CH_3CN); direct current voltage: 30 V; Nafion: 400-μm width and 45-μm depth; miRNA-21 concentration: 1 nM; electrokinetic signal amplification time: 30 min.

3.4. Effects of Nafion membrane dimensions

As a highly negatively charged nanoporous material, Nafion maintains its cation permselectivity. The ICP effect induced by Nafion is one of the most efficient ways to pre-concentrate low abundant molecules [34]. We hypothesized that the stacking efficiency of the ESA system was up to the area of the Nafion membrane (defined by width and depth). To identify how Nafion membrane dimensions affected sensitivity, different membrane widths and depths were investigated. Ion depletion zone length and fluorescence intensity increased by increasing membrane width and depth. However, fluorescence intensity decreased dramatically when membrane width and depth were greater than 400 and 45 μm, respectively (Figs. 3C and D). We hypothesized that when Nafion membrane width and depth were decreased, microchannel conductivity was more dominant than Nafion and formed a shorter depletion zone, resulting in sample leakage [36]. A larger Nafion membrane generated a fast vortical motion and a longer depletion zone which reduced the enrichment efficiency. Considering this, a Nafion membrane with width and depth dimensions of 400 and 45 μm, respectively, was finally chosen.

3.5. ESA system specificity for miRNA-21 detection

Specificity is vital for the real application of the FSNA-ESA system. FSNA-ESA selectivity for miRNA-21 was tested under different conditions, including blank control, 10 nM non-complementary sequences (miRNA-141 and miRNA-375), 10 nM random RNA, 10 nM single-base mismatch (mis-1), and 1 nM miRNA-21. Only miRNA-21 induced a considerable increase in fluorescence intensity, whereas the fluorescence intensity of mis-1 was much lower than of miRNA-21 (Fig. 4A). These results indicate that our system is significantly specific for miRNA-21, which is primarily attributed to molecular hybridization.

3.6. Method validation

Under optimal conditions, linearity was measured by assessing the relationship between fluorescence intensity ($F–F_0$) and the natural logarithm of miRNA-21 concentrations in the range of $1 \times 10^1–5 \times 10^4$ pM . Fluorescence enrichment bands and the miRNA-21 calibration curve are shown (Fig. 4B). Good linearity ($r = 0.9947$) and repeatability (relative standard deviation values were 3.1% and 4.0% for intraday ($n = 6$) and inter-day analyses ($n = 6$), respectively) were obtained for miRNA-21. The limit of detection (LOD) (S/N = 3) was 1.3 pM, which was calculated using the equation: LOD = 3 × SD/k (SD = standard deviation of the blank determination ($n = 11$) and k = slope of the linear regression curve). Our results and data from previous studies were also compared (Table 1)

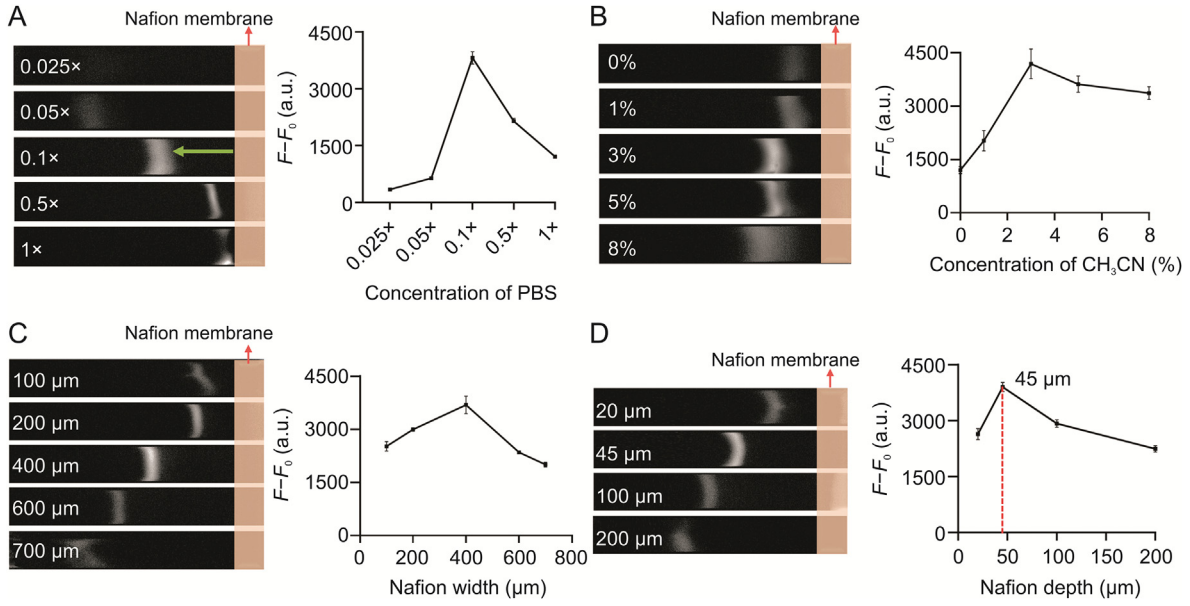

Fig. 3. (A) Effect of phosphate buffered saline (PBS) concentration on fluorescence intensity (green arrow: the depletion region). (B) Effect of CH_3CN concentration on fluorescence intensity. (C) The fluorescence electrokinetic signal amplification (ESA) band depends on Nafion width. (D) The fluorescence ESA band depends on Nafion depth. Conditions: polyA length: 30 nt; molar ratio of polyA 30-DNA and gold nanoparticle (AuNP), 200:1; other conditions as for Fig. 2.

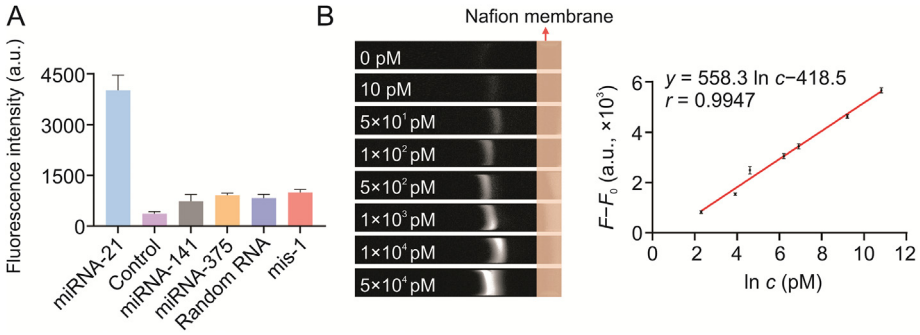

Fig. 4. (A) Specificity validation by the blank control, 10 nM non-complementary sequences microRNAs (miRNA-141 and miRNA-375), 10 nM random RNA, 10 nM single-base mismatch miRNA-21 (mis-1), and 1 nM miRNA-21. (B) Fluorescence intensities responding to different miRNA-21 concentrations.

Table 1
The comparison of different methods for miRNA detection.

Detection platform	Method	Limit of detection (pM)	Linear range (nM)	Refs.
Thiolated DNA probes	Fluorescence	680.0	0–30	[30]
DNA walker	Fluorescence	8.9	0.02–2.5	[31]
Polyadenine-mediated fluorescent spherical nucleic acids	Fluorescence	310.0	0–30	[33]
Lateral flow test	Visual	68.0	0.1–10	[37]
DNA strand displacement	Fluorescence	1.0	0.2–25	[38]
Layered graphene	Electrochemistry	14.6	0.01–100	[39]
Microfluidic electrokinetic enrichment	Fluorescence	1.3	0.01–50	This work

Table 2
Spiked results of miRNA-21 in 1% human serum and 1% human urine matrix.

Samples	Spiked (pM)	Found (pM)	Recovery (%)	Average recovery (%)	Relative standard deviation (%)
Serum	75	85	113.3	108.0	1.7
	750	780	104.0		3.9
	7500	8010	106.8		3.5
Urine	75	81	108.0	106.5	4.1
	750	800	106.7		3.9
	7500	7868	104.9		2.1

[30,31,33,37–39] and indicated relatively better sensitivity and a lower LOD for our method. Furthermore, to explore the applicability of our system, miRNA-21 levels in human serum and a urine matrix were detected. As shown in Table 2, miRNA-21 recoveries in 1% human serum and 1% urine samples were 104.0%–113.3% and 104.9%–108.0%, respectively, and were acceptable [40]. These results suggested our method worked well with complex matrices and showed great promise for early clinical diagnostics.

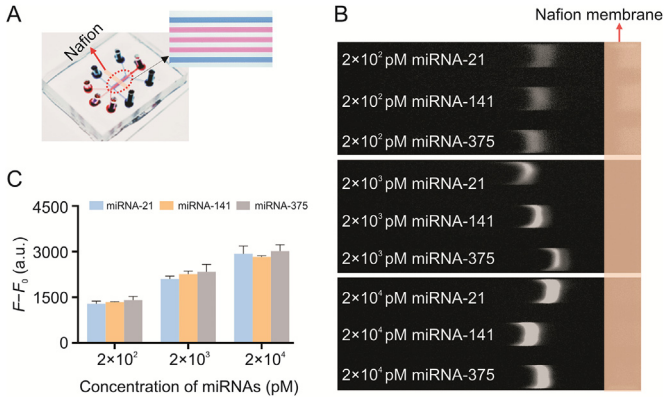

Fig. 5. Schematic presenting the parallel detection of three microRNAs (miRNAs) by the fluorescent spherical nucleic acid-electrokinetic signal amplification system. (A) Image of a three parallel channel microchip. Sample and buffer channels are filled with red and blue dyes, respectively. (B) Three miRNAs with concentrations of 2×10^2–2×10^4 pM accumulated in parallel channels. (C) Fluorescence intensity analyses of samples in Fig. 5B.

3.7. TPC biochip for the simultaneous detection of three miRNAs

As shown in Fig. 5A, the TPC chip comprised three parallel channels (red lines) for online sample enrichment, and the two channels (blue lines) at the side for buffers. Further, miRNA-21, miRNA-141, and miRNA-375 were selected to verify TPC biochip feasibility. As shown in Figs. 5B and C, miRNA fluorescence intensities ($F-F_0$) were enhanced in the TPC biochip in 30 min ESA. Based on these results, our biochip FSNA-ESA system showed excellent potential of simultaneously detecting multiple disease-related miRNAs in clinical samples.

4. Conclusions

We developed a programmable, highly efficient, and homogeneous miRNA detection system based on polyA-mediated FSNAs and an ESA microchip. We demonstrated higher sensitivity compared with previous FSNA sensors. The system LOD was 1.3 pM. Additionally, non-specific adhesion effects were eliminated by simply modulating polyA tail length which favored molecular hybridization. Significantly, our new method is universal, so different miRNAs or DNAs can be detected by altering polyA-DNA recognition sequences. Furthermore, a TPC biochip was used to simultaneously detect three different miRNAs (miRNA-21, miRNA-141, and miRNA-375) related to prostate cancer, and was confirmed as an attractive method of improving sample throughput. Considering these advantages, our method showed great potential as a routine tool for miRNA analysis in disease diagnostics and clinical settings.

CRediT author statement

Jun Xu: Methodology, Validation, Software, Data curation, Investigation, Writing - Original draft preparation; **Qing Tang**: Methodology, Validation; **Runhui Zhang**: Validation; **Haoyi Chen**: Software; **Bee Luan Khoo**, **Xinguo Zhang** and **Yue Chen**: Writing -

Reviewing and Editing, Data curation; **Hong Yan**: Investigation; Methodology; **Jincheng Li**: Software; **Huaze Shao**: Data curation, Formal analysis; **Lihong Liu**: Conceptualization, Methodology, Supervision, Funding acquisition, Resources, Writing - Reviewing and Editing.

Declaration of competing interest

The authors declare that there are no conflicts of interest.

Acknowledgments

This work was supported financially by the National Natural Science Foundation of China (Grant No.: 81973282); Guangdong Basic and Applied Basic Research Foundation (Grant Nos.: 2018A030313843 and 2021A1515011493); National College Students Innovation and Entrepreneurship Training Program (Grant No.: 202012121024); Science and Technology Innovation Strategic Special Project of Guangdong Province ("Climbing Program" Special Project; Grant No.: pdjh2022b0106); Guangdong College Students Innovation and Entrepreneurship Training Program (Grant No.: S202112121154).

Appendix A. Supplementary data

Supplementary data to this article can be found online at https://doi.org/10.1016/j.jpha.2022.05.009.

References

[1] M.M. Fidler, F. Bray, I. Soerjomataram, The global cancer burden and human development: A review, Scand. J. Public Health 46 (2018) 27–36.
[2] P. Vychytilova-Faltejskova, L. Radova, M. Sachlova, et al., Serum-based microRNA signatures in early diagnosis and prognosis prediction of colon cancer, Carcinogenesis 37 (2016) 941–950.
[3] J. Ye, M. Xu, X. Tian, et al., Research advances in the detection of miRNA, J. Pharm. Anal. 9 (2019) 217–226.
[4] P. Pidíkova, R. Reis, I. Herichova, miRNA clusters with down-regulated expression in human colorectal cancer and their regulation, Int. J. Mol. Sci. 21 (2020), 4633.
[5] Y.-H. Zhang, M. Jin, J. Li, et al., Identifying circulating miRNA biomarkers for early diagnosis and monitoring of lung cancer, Biochim. Biophys. Acta Mol. Basis Dis. 1866 (2020), 165847.
[6] B.J. Petri, C.M. Klinge, Regulation of breast cancer metastasis signaling by miRNAs, Cancer Metastasis Rev. 39 (2020) 837–886.
[7] I. Abramovic, M. Ulamec, A. Katusic Bojanac, et al., miRNA in prostate cancer: Challenges toward translation, Epigenomics 12 (2020) 543–558.
[8] E. Várallyay, J. Burgyán, Z. Havelda, MicroRNA detection by northern blotting using locked nucleic acid probes, Nat. Protoc. 3 (2008) 190–196.
[9] E.A. Hunt, D. Broyles, T. Head, et al., MicroRNA detection: Current technology and research strategies, Annu. Rev. Anal. Chem. 8 (2015) 217–237.
[10] L. Li, J. Feng, Y. Fan, et al., Simultaneous imaging of Zn^{2+} and Cu^{2+} in living cells based on DNAzyme modified gold nanoparticle, Anal. Chem. 87 (2015) 4829–4835.
[11] Y. Yang, J. Huang, X. Yang, et al., Aptazyme-gold nanoparticle sensor for amplified molecular probing in living cells, Anal. Chem. 88 (2016) 5981–5987.
[12] M. Bahram, T. Madrakian, S. Alizadeh, Simultaneous colorimetric determination of morphine and ibuprofen based on the aggregation of gold nanoparticles using partial least square, J. Pharm. Anal. 7 (2017) 411–416.
[13] P. Liang, J. Canoura, H. Yu, et al., Dithiothreitol-regulated coverage of oligonucleotide-modified gold nanoparticles to achieve optimized biosensor performance, ACS Appl. Mater. Interfaces 10 (2018) 4233–4242.
[14] H. Pei, F. Li, Y. Wan, et al., Designed diblock oligonucleotide for the synthesis of spatially isolated and highly hybridizable functionalization of DNA-gold nanoparticle nanoconjugates, J. Am. Chem. Soc. 134 (2012) 11876–11879.
[15] D. Zhu, H. Pei, J. Chao, et al., Poly-adenine-based programmable engineering of gold nanoparticles for highly regulated spherical DNAzymes, Nanoscale 7 (2015) 18671–18676.
[16] A. Opdahl, D.Y. Petrovykh, H. Kimura-Suda, et al., Independent control of grafting density and conformation of single-stranded DNA brushes, Proc. Natl. Acad. Sci. U S A 104 (2006) 9–14.
[17] S.M. Schreiner, D.F. Shudy, A.L. Hatch, et al., Controlled and efficient hybridization achieved with DNA probes immobilized solely through preferential DNA-substrate interactions, Anal. Chem. 82 (2010) 2803–2810.
[18] L. Chen, J. Chao, X. Qu, et al., Probing cellular molecules with polyA-based engineered aptamer nanobeacon, ACS Appl. Mater. Interfaces 9 (2017) 8014–8020.
[19] M. Hu, C. Yuan, T. Tian, et al., Single-step, salt-aging-free, and thiol-free freezing construction of AuNP-based bioprobes for advancing CRISPR-based diagnostics, J. Am. Chem. Soc. 142 (2020) 7506–7513.
[20] N. Khandan-Nasab, S. Askarian, A. Mohammadinejad, et al., Biosensors, microfluidics systems and lateral flow assays for circulating microRNA detection: A review, Anal. Biochem. 633 (2021), 114406.
[21] Y. Yang, E. Kannisto, S.K. Patnaik, et al., Ultrafast detection of exosomal RNAs via cationic lipoplex nanoparticles in a micromixer biochip for cancer diagnosis, ACS Appl. Nano Mater. 4 (2021) 2806–2819.
[22] R. Gao, Z. Lv, Y. Mao, et al., SERS-based pump-free microfluidic chip for highly sensitive immunoassay of prostate-specific antigen biomarkers, ACS Sens. 4 (2019) 938–943.
[23] C. Wang, Y. Wang, Y. Zhou, et al., High-performance bioanalysis based on ion concentration polarization of micro-/nanofluidic devices, Anal. Bioanal. Chem. 411 (2019) 4007–4016.
[24] L.S. Cheung, X. Wei, D. Martins, et al., Rapid detection of exosomal microRNA biomarkers by electrokinetic concentration for liquid biopsy on chip, Biomicrofluidics 12 (2018), 014104.
[25] W. Ouyang, S.H. Ko, D. Wu, et al., Microfluidic platform for assessment of therapeutic proteins using molecular charge modulation enhanced electrokinetic concentration assays, Anal. Chem. 88 (2016) 9669–9677.
[26] J. Niu, X. Hu, W. Ouyang, et al., Femtomolar detection of lipopolysaccharide in injectables and serum samples using aptamer-coupled reduced graphene oxide in a continuous injection-electrostacking biochip, Anal. Chem. 91 (2019) 2360–2367.
[27] L. Shi, W. Liu, B. Li, et al., Multichannel paper chip-based gas pressure bioassay for simultaneous detection of multiple microRNAs, ACS Appl. Mater. Interfaces 13 (2021) 15008–15016.
[28] J. Liu, Y. Lu, Preparation of aptamer-linked gold nanoparticle purple aggregates for colorimetric sensing of analytes, Nat. Protoc. 1 (2006) 246–252.
[29] T.L. Halo, K.M. McMahon, N.L. Angeloni, et al., NanoFlares for the detection, isolation, and culture of live tumor cells from human blood, Proc. Natl. Acad. Sci. U S A 111 (2014) 17104–17109.
[30] L.-Y. Zhai, M.-X. Li, W.-L. Pan, et al., *In situ* detection of plasma exosomal microRNA-1246 for breast cancer diagnostics by a Au nanoflare probe, ACS Appl. Mater. Interfaces 10 (2018) 39478–39486.
[31] D. Li, Z. Luo, H. An, et al., Poly-adenine regulated DNA density on AuNPs to construct efficient DNA walker for microRNA-21 detection, Talanta 217 (2020), 121056.
[32] J.H. Lee, Y.-A. Song, J. Han, Multiplexed proteomic sample preconcentration device using surface-patterned ion-selective membrane, Lab Chip 8 (2008) 596–601.
[33] D. Zhu, D. Zhao, J. Huang, et al., Poly-adenine-mediated fluorescent spherical nucleic acid probes for live-cell imaging of endogenous tumor-related mRNA, Nanomedicine 14 (2018) 1797–1807.
[34] S.J. Kim, S.H. Ko, K.H. Kang, et al., Direct seawater desalination by ion concentration polarization, Nat. Nanotechnol. 5 (2010) 297–301.
[35] Z.K. Shihabi, Transient pseudo-isotachophoresis for sample concentration in capillary electrophoresis, Electrophoresis 23 (2002) 1612–1617.
[36] S.H. Ko, Y.-A. Song, S.J. Kim, et al., Nanofluidic preconcentration device in a straight microchannel using ion concentration polarization, Lab Chip 12 (2012) 4472–4482.
[37] W. Zheng, L. Yao, J. Teng, et al., Lateral flow test for visual detection of multiple microRNAs, Sensor. Actuator. B Chem. 264 (2018) 320–326.
[38] R. Chinnappan, R. Mohammed, A. Yaqinuddin, et al., Highly sensitive multiplex detection of microRNA by competitive DNA strand displacement fluorescence assay, Talanta 200 (2019) 487–493.
[39] C.-H. Huang, T.-T. Huang, C.-H. Chiang, et al., A chemiresistive biosensor based on a layered graphene oxide/graphene composite for the sensitive and selective detection of circulating miRNA-21, Biosens. Bioelectron. 164 (2020), 112320.
[40] R. Salahandish, A. Ghaffarinejad, E. Omidinia, et al., Label-free ultrasensitive detection of breast cancer miRNA-21 biomarker employing electrochemical nano-genosensor based on sandwiched AgNPs in PANI and N-doped graphene, Biosens. Bioelectron. 120 (2018) 129–136.